Time-dependent quantum description of molecular double-core-hole-state formation: Impact of the nuclear dynamics on sequential two-photon processes

S. Oberli, N. Sisourat, P. Selles, S. Carniato

Time-dependent quantum description of molecular double core hole states formation: Impact of the nuclear dynamics on sequential two-photon processes

S. Oberli, N. Sisourat, P. Selles and S. Carniato

Laboratoire de Chimie Physique-Matière et Rayonnement,

UMR 7614, Sorbonne Université, UPMC Université Paris 6,

11 rue Pierre et Marie Curie, 75231 Paris Cedex 05, France

(Dated: December 20, 2017)

Abstract

We present a theoretical model to investigate double core hole states formation in molecules through sequential absorption of two x-ray photons from a femtosecond laser pulse. A complete time-dependent quantum description taking into account x-ray absorption and nuclear dynamics explicitly and Auger decay phenomenologically is established within the local approximation. Using this model, we assess the impact of the nuclear dynamics on double core photoionization processes in the case of the carbon monoxide molecule. We show that sequential absorption of two x-ray photons modifies significantly the vibrational distribution of the photoelectron spectra of the double core hole states compared to direct single x-ray photon absorption. Depending on the shape of the potential energy curves involved in the sequential absorption processes, lower or higher vibrational levels may be favoured. Furthermore, in case the final state is dissociative, the electron spectrum is further broaden and blue-shifted in the two-photon process.

I. INTRODUCTION

The unprecedented radiation intensity of x-ray free electron lasers (XFELs) offers the possibility to create double core hole (DCH) states with a single femtosecond pulse via sequential two-photon absorption [1, 2]. This new spectroscopic tool, called x-ray two-photon photoelectron spectroscopy (XTPPS) [3], involves the absorption of a first photon, producing a single core hole (SCH) state with one electron vacancy in the K shell and the emission of a photoelectron. Different pathways are then accessible for the cationic species. It can deexcite radiatively or through the emission of an Auger electron which is the dominant process for light elements [4]. On the other hand, the cation may absorb a second photon leading to the formation of a DCH state. The two core holes are either located on the same atom (single-site DCH) or on different atomic sites (two-site DCH).

Due to the very recent development of XFELs, only few observations of DCH states have been carried out. Most investigations concern atoms [2, 5–9], or multiply core ionized small molecules [10–16].

DCH states can also be produced in synchrotron experiments through single x-ray photon absorption followed by the simultaneous ejection of two electrons [17–19]. However, since double ionization events produced by the absorption of a unique photon entirely depends on electronic correlations, the cross sections are low. Furthermore, in such processes the cross sections for two-site DCH states are orders of magnitude smaller than for single-site DCH states.

On the theoretical side, the first studies on DCH states formation were limited to the calculation of the binding energies of SCHs, single-site and two-site DCHs. These computations were realized at different levels of theory, for example using second order algebraic-diagrammatic constructions - ADC(2) [20–22], the Green's function formalism [23], the complete active space self consistent field (CASSCF) and density

functional theory (DFT) methods [24–28], as well as post Hartree-Fock configuration interaction formalisms [29, 30].

Time-dependent treatments are more delayed, and usually limited to classical rate-equation models describing the time evolution in the different ionization pathways [1–3, 5, 15, 31–34]. However, a complete time-dependent quantum description of DCH states creation in molecules is still missing.

In the present work, we assess for the first time the influence of the nuclear motion on the dynamics of DCH states formation induced by the sequential absorption of two x-ray photons from a single femtosecond laser pulse. For this purpose, a time-dependent quantum treatment of the nuclear motion accompanying x-ray absorption and taking into account phenomenologically the Auger decay is established. This quantum model is applied here to the prototype carbon monoxide (CO) molecule which was investigated in several major experimental and theoretical studies [11, 17, 24, 28, 35]. Studies of single- and two-site doubly core ionized CO molecules formed through single-photon absorption are reported in Refs. [17, 28]. Two-site DCH states of CO produced upon sequential two-photon absorption using XFEL pulses were identified for the first time by Berrah and coworkers [11].

The outline of the paper is as follows: In Sec. II we present the full quantum model to describe DCH states formation. In Sec. III numerical details on the calculations of the ab initio potential energy curves of SCH and DCH states of CO as well as on the nuclear wave packet propagation algorithm are provided. The impact of the nuclear dynamics on core photoionization processes for the different ionization pathways is discussed in Sec. IV. More specifically, the photoelectron spectra of DCH states created either by single-photon absorption or by sequential absorption of two x-ray photons are compared, together with the spectra obtained by neglecting the nuclear motion. Finally in Sec. V we draw conclusions on the study.

II. QUANTUM MODEL TO DESCRIBE DOUBLE CORE HOLE STATES FORMATION

In this section, we consider the dynamics of formation of DCH states through the sequential absorption of two x-ray photons, which is the dominant process in the XFEL regime. Atomic units are used throughout the article unless stated otherwise.

A. Equations of motion

The impact of the nuclear motion on the dynamics of SCH and DCH states formation is investigated by solving the time-dependent Schrödinger equation (TDSE) for the total wave packet

$$\left(\hat{H} + \hat{W}(t)\right) |\Psi(t)\rangle = \mathrm{i}\frac{\mathrm{d}}{\mathrm{d}t} |\Psi(t)\rangle \,. \tag{1}$$

$\hat{H}$ is the unperturbed Hamiltonian given by the sum of the nuclear kinetic energy $\hat{T}$ and the electronic Hamiltonian $\hat{h}_{\mathrm{e}}$. $\hat{W}(t)$ describes the interaction of the molecule with the laser pulse. Within the Born-Oppenheimer formalism, the total wave packet $|\Psi(t)\rangle$ is expanded as:

$$\begin{aligned} |\Psi(t)\rangle = |\chi_{\mathrm{GS}}(t)\rangle \otimes |\mathrm{GS}\rangle + \sum_i \int \mathrm{d}\vec{k}\, |\chi_{\mathrm{SCH}_i}(\vec{k},t)\rangle \otimes |\mathrm{SCH}_i, \vec{k}\rangle\, e^{-\mathrm{i}(\varepsilon+\omega_i)t} \\ + \sum_{i,j,S} \int\int \mathrm{d}\vec{k}\mathrm{d}\vec{k'}\, |\chi^S_{\mathrm{DCH}_{ij}}(\vec{k},\vec{k'},t)\rangle \otimes |\mathrm{DCH}^S_{ij}, \vec{k}\vec{k'}\rangle\, e^{-\mathrm{i}(\varepsilon+\varepsilon'+\omega^S_{ij})t}. \end{aligned} \tag{2}$$

$|\mathrm{GS}\rangle$, $|\mathrm{SCH}_i, \vec{k}\rangle$ and $|\mathrm{DCH}^S_{ij}, \vec{k}\vec{k'}\rangle$ are the ground, the intermediate and the final electronic states, produced by the absorption of two photons successively. The momenta of the two photoelectrons are $\vec{k}$ and $\vec{k'}$, and their energies are ε and ε'. The vertical electronic energies are denoted ω_i for the SCH states and ω^S_{ij} for the

DCH states, where S denotes the spin of the DCH states. $|\chi_{\mathrm{GS}}(t)\rangle$, $|\chi_{\mathrm{SCH}_i}(\vec{k},t)\rangle$ and $|\chi^S_{\mathrm{DCH}_{ij}}(\vec{k},\vec{k'},t)\rangle$ are the nuclear wave packets associated with the ground, the SCH and the DCH states, respectively. Satellite states are not considered in the present work even if they can be found in the same energy region as DCH resonances [10, 13, 36], because they can be circumvented by measuring in coincidence the two photoelectrons.

The interactions between the photoelectrons and the remaining bounded electrons or between the photoelectrons produced in each step are neglected in our model. Thus the first ejected photoelectron is a spectator for the second photoionization event. The order of the indices i and j in the quantities relative to the DCH states is meaningful. Indeed, in the case of CO, a couple (i,j) arranged in that order, indicating a first ionization on the atom i and a second ionization on the atom j, is related to a unique couple of photoelectron energies $(\varepsilon,\varepsilon')$. Moreover, the $(\varepsilon,\varepsilon')$ couples are well separated in all cases, such that quantum interferences between two different pathways leading to the same CO DCH state are negligible.

Within these approximations, a set of coupled time-differential equations is obtained for the nuclear wave packets after integration over the electronic degrees of freedom:

$$\mathrm{i}\frac{\mathrm{d}}{\mathrm{d}t}|\chi_{\mathrm{GS}}(t)\rangle = \hat{h}_{\mathrm{GS}}|\chi_{\mathrm{GS}}(t)\rangle + \sum_i \int \mathrm{d}\vec{k}\; W^*_{gi}(\vec{k},\vec{R},t)e^{-\mathrm{i}(\varepsilon+\omega_i)t}|\chi_{\mathrm{SCH}_i}(\vec{k},t)\rangle \tag{3}$$

$$\begin{aligned}\mathrm{i}\frac{\mathrm{d}}{\mathrm{d}t}|\chi_{\mathrm{SCH}_i}(\vec{k},t)\rangle &= \left(\hat{h}_{\mathrm{SCH}_i} - \frac{\mathrm{i}}{2}\hat{\Gamma}_{\mathrm{SCH}_i} - \omega_i\right)|\chi_{\mathrm{SCH}_i}(\vec{k},t)\rangle + W_{gi}(\vec{k},\vec{R},t)e^{\mathrm{i}(\varepsilon+\omega_i)t}|\chi_{\mathrm{GS}}(t)\rangle \\ &\quad + \sum_{j,S}\int \mathrm{d}\vec{k'}\; W^*_{ijS}(\vec{k'},\vec{R},t)e^{-\mathrm{i}(\varepsilon'+\omega^S_{ij}-\omega_i)t}|\chi^S_{\mathrm{DCH}_{ij}}(\vec{k},\vec{k'},t)\rangle \end{aligned}\tag{4}$$

$$\begin{aligned}\mathrm{i}\frac{\mathrm{d}}{\mathrm{d}t}|\chi^S_{\mathrm{DCH}_{ij}}(\vec{k},\vec{k'},t)\rangle &= \left(\hat{h}^S_{\mathrm{DCH}_{ij}} - \frac{\mathrm{i}}{2}\hat{\Gamma}^S_{\mathrm{DCH}_{ij}} - \omega^S_{ij}\right)|\chi^S_{\mathrm{DCH}_{ij}}(\vec{k},\vec{k'},t)\rangle \\ &\quad + W_{ijS}(\vec{k'},\vec{R},t)e^{\mathrm{i}(\varepsilon'+\omega^S_{ij}-\omega_i)t}|\chi_{\mathrm{SCH}_i}(\vec{k},t)\rangle\,. \end{aligned}\tag{5}$$

The nuclear Hamiltonians for the ground state, the SCH_i state with a core hole on atom i, and the DCH_{ij}^S states with a spin S and two core holes made successively on atom i then on atom j, are given by $\hat{h}_{\rm GS}$, $\hat{h}_{{\rm SCH}_i}$ and $\hat{h}^S_{{\rm DCH}_{ij}}$, respectively. The population leakage of SCH and DCH states due to the finite core hole lifetimes is described phenomenologically through the complex potential terms $\hat{\Gamma}_{{\rm SCH}_i}$ and $\hat{\Gamma}_{{\rm DCH}^S_{ij}}$, respectively [37]. Here $\hat{\Gamma}_{{\rm CH}_i}$ is taken to be the Auger decay width of the $i^{\rm th}$ electronic state because in light atoms Auger decay dominates over radiative relaxation.

The sum over i in Eq. 3 covers the carbon and oxygen SCH states. In Eq. 4, the sum over j spans single-site DCH states as well as singlet and triplet two-site DCH states. Considering a single active electron and approximating the electronic wavefunction by an atomic 1s orbital, the transition matrix elements are given by

$$\begin{aligned} W_{gi}(\vec{k},\vec{R},t) &= \langle {\rm SCH}_i,\vec{k}|\hat{W}(t)|{\rm GS}\rangle \simeq \langle \vec{k}|\hat{W}(t)|1{\rm s}_i\rangle \,\langle {\rm SCH}_i|\hat{a}_{1{\rm s}_i}{\rm GS}\rangle \\ W_{ijS}(\vec{k'},\vec{R},t) &= \langle {\rm DCH}^S_{ij},\vec{k}\vec{k'}|\hat{W}(t)|{\rm SCH}_i,\vec{k}\rangle \simeq \langle \vec{k'}|\hat{W}(t)|1{\rm s}_{j/i}\rangle \,\langle {\rm DCH}^S_{ij}|\hat{a}_{1{\rm s}_{j/i}}{\rm SCH}_i\rangle \,, \end{aligned} \tag{6}$$

where $\hat{a}_{1{\rm s}_i}$ is the operator for the annihilation of an electron in the 1s orbital of the atom i and $\hat{a}_{1{\rm s}_{j/i}}$ is the operator for the annihilation of an electron in the 1s orbital of the atom j in the presence of an electron vacancy in the 1s orbital of the atom i. The photoelectron energies considered here amount to several hundreds of eV, such that photoelectrons can be described as plane waves. Moreover, the matrix elements are evaluated in the frozen orbital approximation [38], taking the overlap integrals equal to one. Dipolar matrix elements normalized per unit energy are derived from the dipolar matrix elements normalized per unit momentum written in equations 6, after a change of variables detailed in the appendix A2. They are calculated in the

velocity gauge (see Ref. [39]) within the rotating wave approximation [38]:

$$\tilde{W}_{ijS}(\varepsilon', t) = -\frac{16\tilde{Z}_{j/i}^{5/2}}{\omega} \sqrt{\frac{n_S \omega \alpha}{3 \text{ FWHM}_\text{t}}} \frac{\sqrt{2\varepsilon'}}{(\tilde{Z}_{j/i}^2 + 2\varepsilon')^2} \frac{1}{2} e^{-2\ln 2\left(\frac{t-t_\text{c}}{\text{FWHM}_t}\right)^2}. \tag{7}$$

In this expression ω is the photon angular frequency, α is the fine structure constant, $\tilde{Z}_{j/i}$ is the effective nuclear charge seen by the $1s_{j/i}$ electron which is removed. According to Slater's rules the following values are taken: $\tilde{Z}_{\text{C/GS}} = \tilde{Z}_{\text{C/O}} = 5.7$, $\tilde{Z}_{\text{O/GS}} = \tilde{Z}_{\text{O/C}} = 7.7$, $\tilde{Z}_{\text{C/C}} = 6$, $\tilde{Z}_{\text{O/O}} = 8$. The laser pulse is described by a sinusoidal electric field linearly polarized along $\hat{z}$ in the laboratory frame, centered at t_c, with a temporal gaussian envelope defined by a full width at half maximum FWHM_t. The laser pulse intensity is defined as $I = n_S \times \omega \times \text{FWHM}_t^{-1}$, with n_S the number of photons per unit surface.

The equations of motion are further simplified by introducing photoionization decay widths derived in the local approximation [40]. These decay widths describe the depopulation of the ground and SCH states induced by photon absorption. Using the change of variables given in appendix A, one obtains the following set of coupled differential equations for the nuclear wavepackets normalized per unit energy:

$$\text{i}\frac{\text{d}}{\text{d}t}\left|\chi_{\text{GS}}(t)\right\rangle = \left(\hat{h}_{\text{GS}} - \frac{\text{i}}{2}\hat{\Gamma}^{\text{photo}}_{\text{GS}\to\text{SCHs}}(t)\right)\left|\chi_{\text{GS}}(t)\right\rangle \tag{8}$$

$$\begin{aligned}\text{i}\frac{\text{d}}{\text{d}t}\left|\tilde{\chi}_{\text{SCH}_i}(\varepsilon, t)\right\rangle = &\left(\hat{h}_{\text{SCH}_i} + \varepsilon - \omega - \frac{\text{i}}{2}\hat{\Gamma}_{\text{SCH}_i} - \frac{\text{i}}{2}\hat{\Gamma}^{\text{photo}}_{\text{SCH}_i\to\text{DCHs}}(t)\right) \\ &\times \left|\tilde{\chi}_{\text{SCH}_i}(\varepsilon, t)\right\rangle + \tilde{W}_{gi}(\varepsilon, t)\left|\chi_{\text{GS}}(t)\right\rangle\end{aligned} \tag{9}$$

$$\begin{aligned}\text{i}\frac{\text{d}}{\text{d}t}\left|\tilde{\chi}^S_{\text{DCH}_{ij}}(\varepsilon, \varepsilon', t)\right\rangle = &\left(\hat{h}^S_{\text{DCH}_{ij}} + \varepsilon + \varepsilon' - 2\omega - \frac{\text{i}}{2}\hat{\Gamma}^S_{\text{DCH}_{ij}}\right)\left|\tilde{\chi}^S_{\text{DCH}_{ij}}(\varepsilon, \varepsilon', t)\right\rangle \\ &+ \tilde{W}_{ijS}(\varepsilon', t)\left|\tilde{\chi}_{\text{SCH}_i}(\varepsilon, t)\right\rangle.\end{aligned} \tag{10}$$

Total photoionization decay widths can be decomposed in partial decay widths, one

for each open core photoionization pathway:

$$\hat{\Gamma}^{\text{photo}}_{\text{GS}\to\text{SCHs}}(t) = \sum_i \hat{\Gamma}^{\text{photo}}_{\text{GS}\to\text{SCH}_i}(t) = 2\pi \sum_i |\tilde{W}_{gi}(t;\varepsilon_i = \omega - \omega_i)|^2, \tag{11}$$

for the ground state, and

$$\hat{\Gamma}^{\text{photo}}_{\text{SCH}_i\to\text{DCHs}}(t) = \sum_{j,S} \hat{\Gamma}^{\text{photo}}_{\text{SCH}_i\to\text{DCH}^S_{ij}}(t) = 2\pi \sum_{j,S} |\tilde{W}_{ijS}(t;\varepsilon^S_{ij} = 2\omega - \omega^S_{ij} - \varepsilon_i)|^2, \tag{12}$$

for the SCH state with a core hole on atom i. ε_i and ε^S_{ij} are the resonant photoelectron energies. For the local approximation to be valid, the transition dipole moments should weakly depend on the photoelectron energy in a large interval around the resonance defined by $[\varepsilon_i - E, \varepsilon_i + E]$ for the first ionization step and by $[\varepsilon^S_{ij} - E, \varepsilon^S_{ij} + E]$ for the second step. Furthermore, the parameter E should be chosen such that $2\pi/E$ is small compared to the pulse duration (see [40] for more details). In our model, the transition dipole moments change by less than 10% within an energy interval of $\pm$ 20 eV around the resonances. Moreover, we consider in this work a pulse duration of 40 fs. Both conditions are therefore satisfied.

The energy differential cross section for the creation of a specific DCH^S_{ij} state and two photoelectrons of energy ε and ε' is (see Ref. [41])

$$\frac{\mathrm{d}^2\sigma^S_{ij}(\varepsilon,\varepsilon')}{\mathrm{d}\varepsilon \mathrm{d}\varepsilon'} = \frac{g}{n_S}\hat{\Gamma}^S_{\text{DCH}_{ij}} \int_{-\infty}^{+\infty} \mathrm{d}t \ \langle \tilde{\chi}^S_{\text{DCH}_{ij}}(\varepsilon,\varepsilon',t) | \tilde{\chi}^S_{\text{DCH}_{ij}}(\varepsilon,\varepsilon',t) \rangle \,. \tag{13}$$

For a one-site process $g = 2$, for a two-site process leading to a singlet state $g = 1$ and for a two-site process leading to a triplet state $g = 3$.

In order to highlight the effects of the nuclear dynamics in the intermediate SCH states, we compare the results from the sequential absorption of two x-ray photons with that from direct single photon absorption. We therefore integrate the doubly differential cross section (Eq. 13) along lines of constant sum of the energies of the

two photoelectrons (i.e. $\varepsilon_T = \varepsilon + \varepsilon' = \text{cte}$). The cross sections obtained through this integration are given by:

$$\frac{\mathrm{d}\sigma_{ij}^{S}(\varepsilon_T)}{\mathrm{d}\varepsilon_T} = \frac{g}{n_S}\hat{\Gamma}^{S}_{\mathrm{DCH}_{ij}} \int_0^{\varepsilon_T} \mathrm{d}\varepsilon \int_{-\infty}^{+\infty} \mathrm{d}t \, \langle \tilde{\chi}^{S}_{\mathrm{DCH}_{ij}}(\varepsilon, \varepsilon_T - \varepsilon, t) | \tilde{\chi}^{S}_{\mathrm{DCH}_{ij}}(\varepsilon, \varepsilon_T - \varepsilon, t) \rangle \, . \tag{14}$$

These cross sections are compared with the following cross sections for the single-photon pathway

$$\frac{\mathrm{d}\sigma_{ij}^{S}(\varepsilon_T)}{\mathrm{d}\varepsilon_T} \propto \int_{-\infty}^{+\infty} \mathrm{d}t \, \langle \chi_{\mathrm{GS}}(t=0) | e^{-\mathrm{i}\hat{h}^{S}_{\mathrm{DCH}_{ij}} t} | \chi_{\mathrm{GS}}(t=0) \rangle \, e^{(\mathrm{i}\varepsilon_T - \hat{\Gamma}^{S}_{\mathrm{DCH}_{ij}})t}, \tag{15}$$

where we assume a direct broadband excitation from the ground electronic state to the DCH state.

III. NUMERICAL DETAILS

A. Ab initio potential energy curves and Auger lifetimes of SCH and DCH states of CO

Potential energy curves (PECs) are calculated for the ground, the SCH as well as the single-site and two-site DCH states at a configuration interaction level of theory including single and double excitations (CISD) to take into account electronic correlations properly. Molecular orbitals are calculated using the Hartree-Fock procedure and include the large relaxation effects upon core ionization [29, 30]. The correlation-consistent polarized valence quadruple-zeta (cc-pVQZ) basis set of Dunning [42] is opted for all states. Calculations are performed with the GAMESS-(US) 2013 program package.

The calculated PECs are shown in Fig. 1. All electronic states have a bound PEC,

Core hole state	Vertical electronic energy [eV]		
	Present	Ref. [24] (Theo.)	Ref. [11] (Exp.)
$[C(K^{-1})O]^{+}$	296.81	296.358	296.5±0.5
$[CO(K^{-1})]^{+}$	542.50	542.820	
$[C(K^{-2})O]^{2+}$	666.11	664.418	667.9±3.6
$[CO(K^{-2})]^{2+}$	1176.00	1176.561	
$[C(K^{-1})O(K^{-1})]^{2+}(S=0)$	855.09	854.743	855.3±1.2
$[C(K^{-1})O(K^{-1})]^{2+}(S=1)$	855.34	855.200	

TABLE I: Vertical electronic energies of SCH (ω_i) and DCH (ω_{ij}^{S}) states of carbon monoxide.

except the oxygen single-site DCH state which exhibits a repulsive PEC. In the case of core-holes on the carbon atom the equilibrium internuclear distance shortens as core electrons are successively removed. In contrast, the equilibrium distance of the singly core ionized oxygen state is larger than that of the ground state. The singlet and triplet two-site DCH states have nearly identical PECs with an equilibrium distance close to the ground state value. Owing to the different shapes of the PECs, distinct effects of the nuclear dynamics are expected for the different two-photon pathways.

The vertical ionization potentials are summarized and compared with values from literature in Table I. Our calculated vertical ionization potentials show a very good agreement with experimental results.

Concerning the Auger lifetimes of SCH states of CO, a range of experimental and theoretical values can be found in the literature [43–51]. In our model the Auger lifetimes of SCH states are taken from Ref. [43]. To our knowledge, no Auger lifetimes of DCH states for CO are reported yet. In this work, the core hole lifetimes of single-site DCH states are taken to be three times smaller than that of SCH states as in Refs. [13, 34, 52]. The decay rate of the two-site DCH state is defined as the sum of the decay rates of the carbon and oxygen SCH states, in

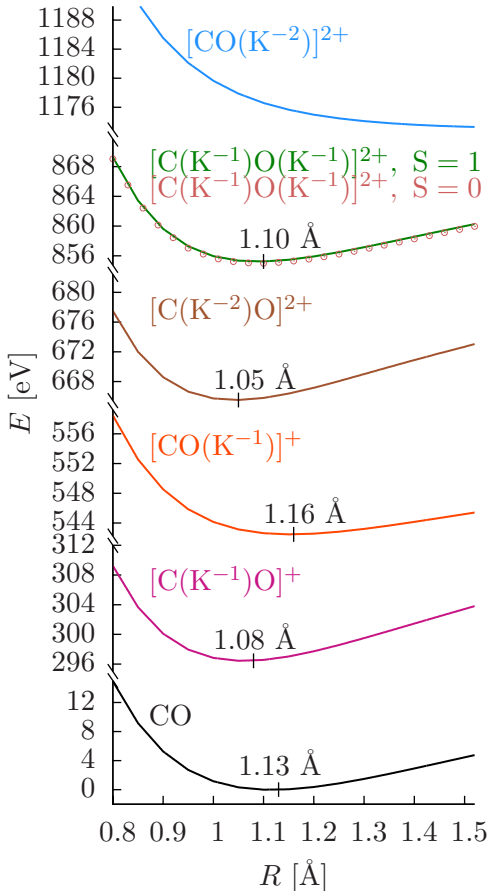

FIG. 1: Ab initio PECs for the ground, SCH, single-site and two-site DCH states of CO, calculated at the CISD level of theory. The equilibrium internuclear distances are indicated for each electronic state.

the approximation of independent core holes. The Auger lifetimes ($\tau_{\rm CH}$) and the corresponding Auger decay widths ($\hat{\Gamma}_{\rm CH} = \hbar/\tau_{\rm CH}$) of the SCH and DCH states of CO used in our calculations are given in Table II.

Core hole state	Auger lifetime τ_{CH} [fs]	Auger decay width $\hat{\Gamma}_{\mathrm{CH}}$ [meV]
$[\mathrm{C}(\mathrm{K}^{-1})\mathrm{O}]^{+}$	6.86	96 [43]
$[\mathrm{CO}(\mathrm{K}^{-1})]^{+}$	3.85	171 [43]
$[\mathrm{C}(\mathrm{K}^{-2})\mathrm{O}]^{2+}$	2.29	288
$[\mathrm{CO}(\mathrm{K}^{-2})]^{2+}$	1.28	513
$[\mathrm{C}(\mathrm{K}^{-1})\mathrm{O}(\mathrm{K}^{-1})]^{2+}(S=0,1)$	2.47	267

TABLE II: Auger lifetimes and decay widths of SCH and DCH states of carbon monoxide.

B. Implementation of the nuclear wave packet propagation

The nuclear wave packet propagation is performed on a spatial grid defined along the internuclear distance within the sine- discrete variable representation (sine-DVR) [53]. In order to obtain the photoelectron coincidence spectra associated with the DCH states, the equations of motion (Eqs. 8-10) are solved for each pair of values (ε,ε') thanks to the fourth-order Runge-Kutta method [54]. Convergence is reached for a spatial grid step $\Delta R = 0.02$ Å, a time step $\Delta t = 10^{-2}$ fs, and a photoelectron energy step of $\Delta\varepsilon = 0.02$ eV. The laser pulse duration is fixed to $\mathrm{FWHM}_t = 40$ fs ($\mathrm{FWHM}_\omega = 91.2$ meV). The initial state is the lowest vibrational state (ν_0) of the ground electronic state. The final time of propagation (240 fs) is chosen such that the populations in the core hole states are smaller than 10^{-7}, i.e. when the electric field is almost zero and when the population leakage due to Auger decay is negligible.

IV. VIBRATIONALLY RESOLVED PHOTOELECTRON SPECTRA OF CO DCH STATES

In the following, we want to assess the impact of the nuclear dynamics on core photoionization processes leading to the formation of CO single-site and two-site

DCH states. A detailed analysis is carried out for each ionization channel separately. The photon energy is chosen at 1 keV such that all ionization channels are open. The number of photons within the single pulse of 40 fs duration is fixed to 4×10^9 for all the calculations. For a laser pulse focusing area of 1.6 μm^2, the photon density is thus $n_S = 4$ Mb^{-1}.

A. Formation of carbon single-site DCH state

We first discuss the formation of carbon single-site DCH state. The corresponding photoelectron-photoelectron coincidence spectrum is shown in the left panel of Fig. 2. The axes ε and ε' correspond to the energy of the photoelectrons produced in the

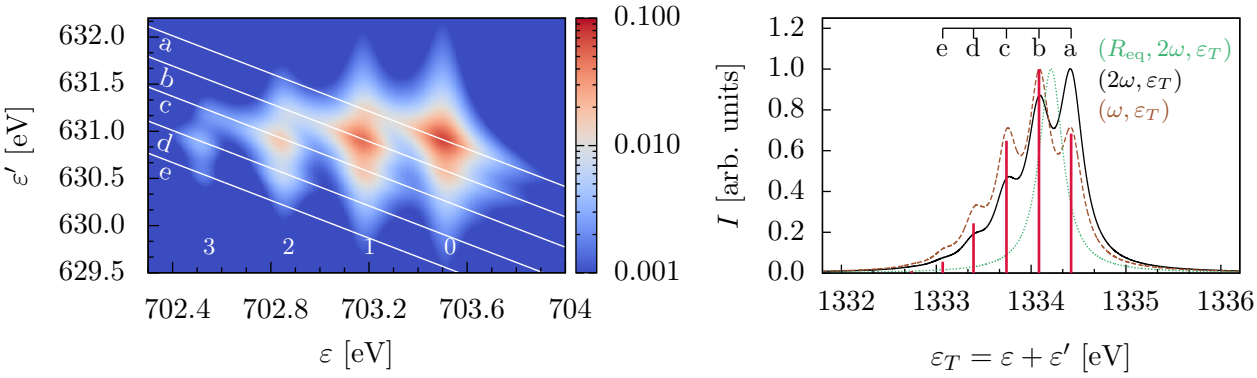

FIG. 2: Left panel: Photoelectron-photoelectron coincidence spectrum for $[C(K^{-2})O]^{2+}$ formation (logarithmic scale in arbitrary units). The labels (0-3) indicate the vibrational level of the SCH state. The labels (a-e) indicate the vibrational level of the DCH state. See text for more details. Right panel: Comparison of the spectra of the total photoelectron energy ε_T. Black full line: Two-photon process including nuclear dynamics; Green dotted line: Two-photon process simulated from vertical transitions at the equilibrium internuclear distance of the ground electronic state; Brown dashed line: One-photon process including nuclear dynamics. The three spectra are scaled with respect to their most intense peak. The red vertical bars correspond to the Franck-Condon factors for the production of each (a-e) vibrational level of the DCH state.

first and second ionization events, respectively. A vertical line corresponds to the formation of a given vibrational state of the SCH state. A vibrational progression is clearly observed: the main contributions of the peaks centered at $\varepsilon \sim 703.51$, 703.18, 702.85 and 702.53 eV are the ν_0^{SCH}, ν_1^{SCH}, ν_2^{SCH} and ν_3^{SCH} vibrational states, respectively (see labels (0-3) at the bottom of the panel). Moreover, each spot along a vertical line is associated with a given vibrational state of the DCH state. On the other hand, a diagonal line corresponds to a given total photoelectron energy $\varepsilon_T = \varepsilon + \varepsilon'$, and thus to the formation of a given vibrational state of the DCH state. The corresponding labels (a-e) indicate the vibrational levels ($0 \rightarrow 4$), and are indicated on the left side of the panel. The main ionization channels leading to the formation of $[\mathrm{C}(\mathrm{K}^{-2})\mathrm{O}]^{2+}$ are summarized in Table III, where the relative intensities with respect to the most probable event are collected. In contrast to the first ionization step, one can not associate a vibrational state to a particular value of ε'. Nevertheless, the vibrational progression in the DCH state is observed when the photoelectron-photoelectron coincidence spectum is integrated along lines of constant ε_T (right panel of Fig. 2).

The differential cross sections with respect to the total photoelectron energy, as defined in Eq. 14 for the sequential two-photon process and in Eq. 15 for the direct one-photon process are displayed in the right panel, as well as the spectrum obtained for a two-photon process at a fixed internuclear distance. In the following, we compare the three spectra in order to highlight the role of the nuclear dynamics on DCH state formation. The spectrum for the sequential two-photon pathway including nuclear dynamics (black full line) – labeled $(2\omega, \varepsilon_T)$ in the following – presents a long vibrational progression corresponding to the population of the five lowest vibrational states in the final DCH state. Several ionization pathways are possible for a given energy ε_T. For example, the peak at 1334.41 eV (label a) mainly originates from the population of the fundamental vibrational level of the SCH intermediate state and

Label	$[C(K^{-2})O]^{2+}$	$[C(K^{-1})O(K^{-1})]^{2+}$ via $[C(K^{-1})O]^{+}$	$[C(K^{-1})O(K^{-1})]^{2+}$ via $[CO(K^{-1})]^{+}$
a	00 (100) 10 (6.82)	00_S (31.0) 10_S (5.05) 20_S (0.19)	00_S (25.6) 10_S (6.86) 20_S (0.52)
b	01 (9.24) 11 (65.1) 21 (4.03)	00_T, 01_S (100) 10_T, 11_S (29.2) 20_T, 21_S (3.61)	00_T, 01_S (100) 10_T, 11_S (20.7) 20_T, 21_S (2.15)
c	12 (12.4) 22 (20.3)	01_T, 02_S (19.5) 11_T, 12_S (52.7) 21_T, 22_S (11.7)	01_T, 02_S (83.5) 11_T, 12_S (5.20) 21_T, 22_S (2.15)
d	13 (0.33) 23 (5.97) 33 (3.74)	02_T, 03_S (2.26) 12_T, 13_S (25.8) 22_T, 23_S (11.9)	02_T, 03_S (34.7) 12_T, 13_S (19.9)
e	-	13_T, 14_S (5.00) 23_T, 24_S (11.4)	03_T, 04_S (8.28) 13_T, 14_S (17.8)
f	-	14_T, 15_S (0.65) 24_T, 25_S (3.32)	04_T, 05_S (1.31) 14_T, 15_S (6.86) 24_T, 25_S (3.12)

TABLE III: Main ionization pathways. The labels (a→f) refer to the vibrational levels (0→5) of the DCH states. Each box in the table contains information on the vibrational levels of the intermediate SCH and final DCH states and on the relative Franck Condon intensities (given in parentheses). The indexes S and T refer to the spin state of the DCH.

to a less extent from that of the first excited vibrational level (see Table III). The pathway via the ground vibrational state dominates although $R_{\rm eq}^{\rm SCH} < R_{\rm eq}^{\rm GS}$, since the shape of the PECs of the ground and SCH states is different. Moreover, the $R_{\rm eq}$ of the SCH and DCH states are close to each other and the corresponding PECs have a similar shape (see Fig. 1), such that the vibrational populations are almost unchanged during the second photon absorption (i.e. $\nu_i^{\rm SCH} \rightarrow \nu_i^{\rm DCH}$ is favoured).
The spectrum obtained for a two-photon process without including the nuclear degree of freedom (green dotted line) – labeled $(R_{\rm eq}, 2\omega, \varepsilon_T)$ – exhibits a single peak with a FWHM of 0.3 eV. The comparison of the $(R_{\rm eq}, 2\omega, \varepsilon_T)$- and $(2\omega, \varepsilon_T)$-spectra

shows that the nuclear dynamics broadens substantially the energy distribution. For this system and a laser pulse of 40 fs, vibrational dynamics is the largest source of broadening.

The spectrum obtained for the direct one-photon pathway (brown dashed line) – labeled (ω, ε_T) – also exhibits a well-resolved vibrational progression. However, the relative intensities of the peaks differ from that of the $(2\omega, \varepsilon_T)$-spectrum. In the case of direct ionization, ν_1^{DCH} is dominantly populated while when the system goes via the SCH intermediate state the most intense peak corresponds to ν_0^{DCH}. The first excited vibrational state is favoured in the former case owing to the shortening of the bond of 0.08 Å accompanying the photon absorption, while in the latter case the dynamics in the intermediate SCH state enhances the population of ν_0^{DCH}. The difference in the relative intensity distributions in the vibrational structure of the spectra for the two-photon and one-photon pathways illustrates the influence of the nuclear dynamics in the intermediate SCH state, and provides information on the shape and the relative displacement of the core hole PECs.

B. Formation of oxygen single-site DCH state

In contrast to the carbon case, the equilibrium bond length increases of 0.03 Å when one core electron is removed from the oxygen 1s orbital. Furthermore, the molecule dissociates after creating a second vacancy in the oxygen K-shell. We therefore expect a completely different impact of the nuclear dynamics during the formation of oxygen single-site DCH state. The photoelectron-photoelectron coincidence spectrum is shown in the left panel of Fig. 3. Three peaks are visible in the spectrum at $\varepsilon \sim 457.54$, 457.32 and 457.06 eV corresponding to the population of ν_0^{SCH}, ν_1^{SCH} and ν_2^{SCH}, respectively. No vibrational distribution is observed along the energy of the second photoelecton due to the dissociative character of the oxygen single-site

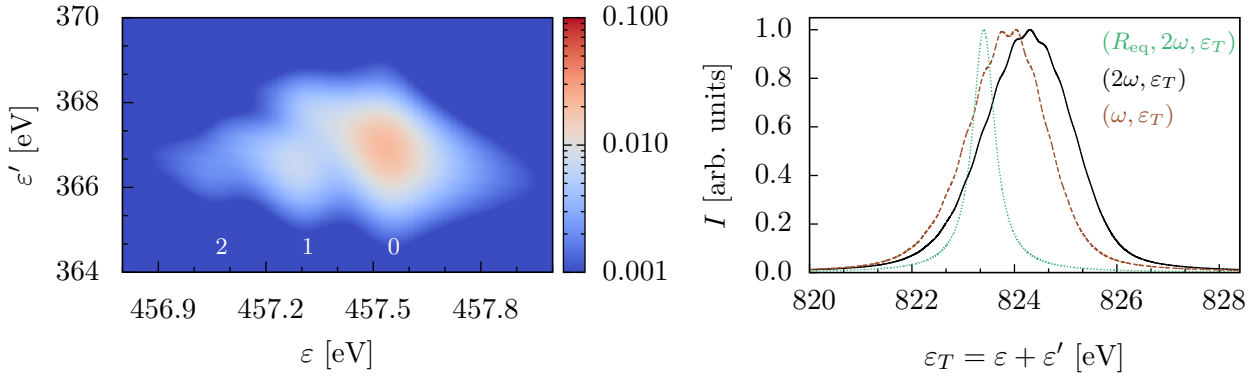

FIG. 3: Left panel: Photoelectron-photoelectron coincidence spectrum of $[CO(K^{-2})]^{2+}$ state (logarithmic scale in arbitrary units). Right panel: Comparison of the spectra of the total photoelectron energy ε_T. For further details on the different spectra, see caption of Fig. 2.

DCH state.

The $(2\omega, \varepsilon_T)$, $(R_{\rm eq}, 2\omega, \varepsilon_T)$ and (ω, ε_T)-spectra are compared in the right panel of Fig. 3. The comparison between the $(2\omega, \varepsilon_T)$- and (ω, ε_T)- spectra with the $(R_{\rm eq}, 2\omega, \varepsilon_T)$-spectrum shows that the vibrational broadening is significant. Again it is ascribed to the dissociative character of $[CO(K^{-2})]^{2+}$. The FWHM of the $(2\omega, \varepsilon_T)$-spectrum amounts to 2 eV which is larger than that of the spectrum for the one-photon absorption (FWHM=1.8 eV). The broadening of the $(2\omega, \varepsilon_T)$-spectrum is due to the spread of the nuclear wave packet along R in the SCH state. Furthermore, the $(2\omega, \varepsilon_T)$-spectrum is shifted by +0.9 eV and by +0.27 eV with respect to the $(R_{\rm eq}, 2\omega, \varepsilon_T)$- and (ω, ε_T)-spectra, respectively. This energy shift is explained by the elongation of the bond in the intermediate SCH state.

C. Formation of two-site DCH states

The contribution of singlet and triplet two-site DCH states superimposed in the electron spectra owing to the small energy difference between these two states. In-

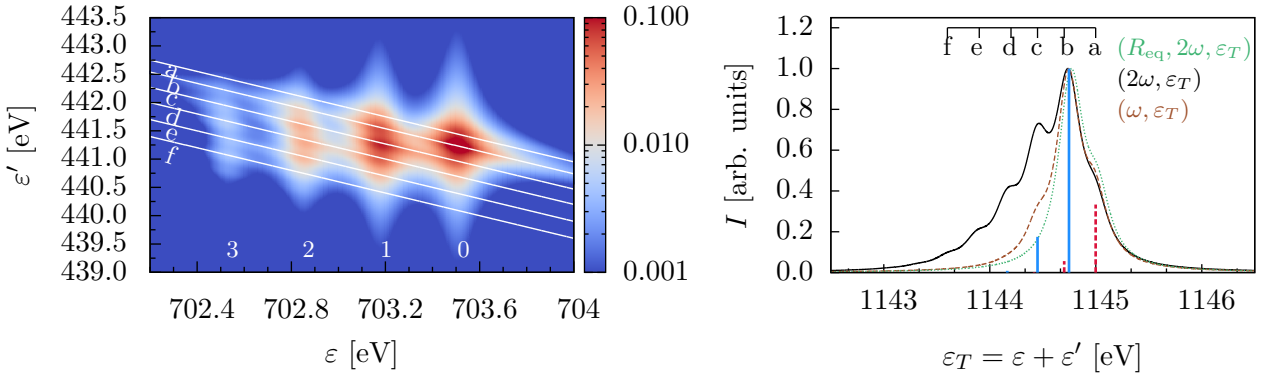

FIG. 4: Left panel: Photoelectron-photoelectron coincidence spectrum of $[C(K^{-1})O(K^{-1})]^{2+}$ state, with $[C(K^{-1})O]^{+}$ as the intermediate SCH state (logarithmic scale in arbitrary units). Right panel: Comparison of the spectra of the total photoelectron energy ε_T. Red dashed and blue full vertical bars: Contributions of the singlet and triplet cationic states, respectively. For further details on the different spectra, see caption of Fig. 2.

deed, the difference in the vertical electronic energies between the triplet and singlet states (251 meV) is in the order of the vibrational energy spacing of the two-site DCH states (297-283 meV). In the following, we therefore show the sum of the two contributions. Each state can be reached by two pathways, either via the carbon SCH or via the oxygen SCH states. However, the energy pairs $(\varepsilon, \varepsilon')$ for the two pathways differ significantly, such that one knows which element is ionized first. The photoelectron-photoelectron coincidence spectra with $[C(K^{-1})O]^{+}$ and $[CO(K^{-1})]^{+}$ as the intermediate SCH states are shown in Fig. 4 and 5, respectively. The main ionization pathways and their relative intensities are summarized in Table III.

The vibrational progressions along ε are similar to that observed in the single-site DCH spectra. However, owing to the different PECs of the two-site DCH states and of the single-site DCH ones, the distributions along ε' are clearly different. The spectrum obtained by integrating the photoelectron-photoelectron coincidence spectrum along diagonal lines is shown in the right panels of the Figs. 4 and 5, together with the

$(R_{\rm eq}, 2\omega, \varepsilon_T)$- and (ω, ε_T)-spectra. We first discuss the spectrum with $[C(K^{-1})O]^+$ as the intermediate SCH state. The (ω, ε_T)- and $(R_{\rm eq}, 2\omega, \varepsilon_T)$-spectra differ only marginally due to the similar shape of the PECs and the close $R_{\rm eq}$ of the ground electronic and two-site DCH states. However, the $(2\omega, \varepsilon_T)$-spectrum exhibits a much longer vibrational distribution than the two latter. Indeed, in the case of two-photon absorption and when the nuclear dynamics is included, vibrational levels up to $\nu_5^{\rm DCH}$ can be reached while only $\nu_0^{\rm DCH}$, $\nu_1^{\rm DCH}$ are seen in the one-photon spectrum. These results show that the nuclear dynamics in the intermediate state allows to reach higher vibrational levels compared to the direct pathway.

Same conclusions are drawn for the pathway via the oxygen SCH state. The difference between the $(2\omega, \varepsilon_T)$-spectra with the carbon and oxygen as intermediate SCH states is shown in the right panel of Fig. 5 (gray area). These normalized spectra are almost identical, since the energy of the intermediate SCH state cancels

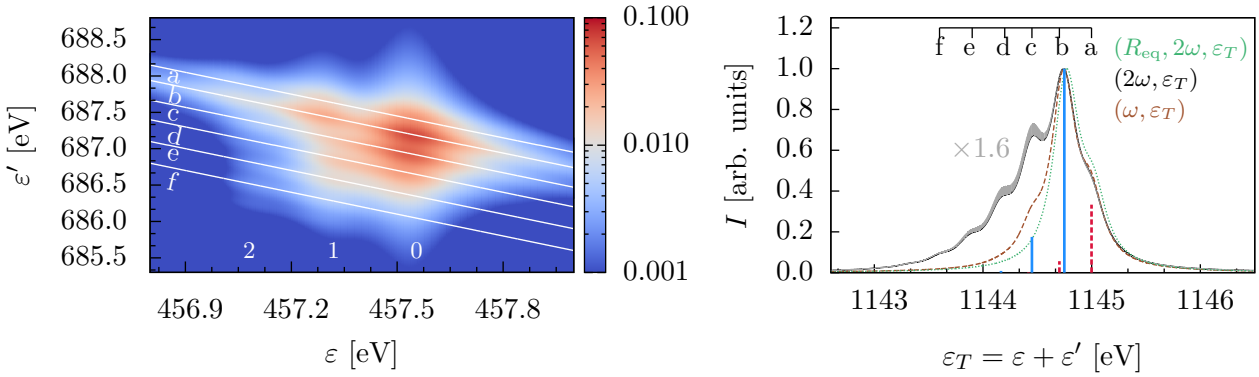

FIG. 5: Left panel: Photoelectron-photoelectron coincidence spectrum of $[C(K^{-1})O(K^{-1})]^{2+}$ state, with $[CO(K^{-1})]^+$ as the intermediate SCH state (logarithmic scale in arbitrary units). Right panel: Comparison of the spectra of the total photoelectron energy ε_T. The difference between the $(2\omega, \varepsilon_T)$-spectra with the carbon and oxygen as intermediate SCH states is given in gray shaded area, together with the scaling factor. Red dashed and blue full vertical bars: Contributions of the singlet and triplet cationic states, respectively. For further details on the different spectra, see caption of Fig. 2.

by energy conservation for the two-photon process. However, there is a small change in the normalized intensity distributions coming from the different transition dipole moments and SCH Auger decay widths. The non-normalized spectrum is 1.6 times more intense for the ionization pathway via the carbon SCH state. Moreover, the vibrational pathways to reach the same vibrational state of the DCH state are different: for example, the main ionization pathways to reach ν_3^{DCH} via $[\mathrm{C}(\mathrm{K}^{-1})\mathrm{O}]^+$ is 013 and 023, while the major contributions come from 003 and 013 when $[\mathrm{CO}(\mathrm{K}^{-1})]^+$ is the intermediate state (see Table III).

To conclude, the photoelectron-photoelectron coincidence spectra of the two-site DCH states are clearly distinguishable for the ionization pathways via $[\mathrm{C}(\mathrm{K}^{-1})\mathrm{O}]^+$ and $[\mathrm{CO}(\mathrm{K}^{-1})]^+$. In contrast, the normalized ε_T-spectra for the two pathways differ only slightly in intensity but the peak positions are identical.

V. CONCLUSIONS

In the present study, the formalism to describe DCH states production through the sequential absorption of two x-ray photons from a femtosecond laser pulse is developed. The intricated problem of x-ray absorption, nuclear dynamics and Auger decay is investigated using a full quantum treatment of both electronic and nuclear motions. This time-dependent quantum model is applied to carbon monoxide, which is used as a prototype molecule. We tackled the study of the influence of the nuclear dynamics on core photoionization processes. In this purpose, the photoelectron coincidence spectra associated with single-site and two-site DCH states of CO are calculated. The kinetic energy distribution of the first emitted photoelectron exhibits a clear vibrational progression, and is a fingerprint of the nuclear dynamics in the intermediate SCH state. The vibrational progression of the DCH states appears in the spectra of the total photoelectron energy. Moreover, a comparison is given be-

tween the sum of the energies of the photoelectrons emitted through the sequential absorption of two x-ray photons (including or neglecting the nuclear motion) and for the direct single-photon pathway. We showed that the signature of the nuclear dynamics is characteristic of the ionization pathway and permits to deduce information on the topologies of the PECs and their relative displacements. In order to investigate DCH spectroscopy for chemical analysis purposes, it would be interesting to extend the present study to higher dimensional systems.

Appendix A: Definitions of nuclear wave packets and transition dipole matrix elements

In order to obtain the time-differential equations of motion in photoelectron energies from those in photoelectron momenta, we perform the following change of variables for the nuclear wave packets

$$\begin{aligned} |\chi_{\mathrm{SCH}_i}(\vec{k},t)\rangle &= |\tilde{\chi}_{\mathrm{SCH}_i}(\varepsilon,t)\rangle\,(2\varepsilon)^{-1/4}Y_{10}(\Omega_k)e^{\mathrm{i}\vec{k}\cdot\overrightarrow{\mathrm{GA}}_i}e^{\mathrm{i}(\varepsilon+\omega_i-\omega)t} \\ |\chi^S_{\mathrm{DCH}_{ij}}(\vec{k},\vec{k'},t)\rangle &= |\tilde{\chi}^S_{\mathrm{DCH}_{ij}}(\varepsilon,\varepsilon',t)\rangle\,(2\varepsilon)^{-1/4}(2\varepsilon')^{-1/4}Y_{10}(\Omega_k)Y_{10}(\Omega_{k'})e^{\mathrm{i}\vec{k}\cdot\overrightarrow{\mathrm{GA}}_i}e^{\mathrm{i}\vec{k'}\cdot\overrightarrow{\mathrm{GA}}_j}e^{\mathrm{i}(\varepsilon+\varepsilon'+\omega^S_{ij}-2\omega)t}, \end{aligned} \tag{A1}$$

and for the transition dipole matrix elements,

$$\begin{aligned} W_{gi}(\vec{k},\vec{R},t) &= \tilde{W}_{gi}(\varepsilon,t)(2\varepsilon)^{-1/4}e^{-\mathrm{i}\omega t}Y_{10}(\Omega_k)e^{\mathrm{i}\vec{k}\cdot\overrightarrow{\mathrm{GA}}_i} \\ W_{ijS}(\vec{k'},\vec{R},t) &= \tilde{W}_{ijS}(\varepsilon',t)(2\varepsilon')^{-1/4}e^{-\mathrm{i}\omega t}Y_{10}(\Omega_{k'})e^{\mathrm{i}\vec{k'}\cdot\overrightarrow{\mathrm{GA}}_j}. \end{aligned} \tag{A2}$$

Ω_k and $\Omega_{k'}$ are the solid angles for the emission of the first and second photoelectrons, resp. The phase $\exp(\mathrm{i}\vec{k}\cdot\overrightarrow{\mathrm{GA}}_i)$ defines the photoelectron momentum $\vec{k}$ with respect

to a common reference for all plane waves. $\overrightarrow{\mathrm{GA}_i}$ is the length vector between the center of mass of the molecule G and the ionized atom A_i. All phases simplify in the equations of motion.

ACKNOWLEDGMENTS

This research was supported by the Swiss National Science Foundation (NSF(CH)) with Doc.Mobility fellowship (Grant No. P1SKP2 168495).

---

[1] N. Rohringer and R. Santra, Physical Review A **76**, 033416 (2007).

[2] L. Young, E. P. Kanter, B. Krässig, Y. Li, A. M. March, S. T. Pratt, R. Santra, S. H. Southworth, N. Rohringer, L. F. DiMauro, *et al.*, Nature **466**, 56 (2010).

[3] R. Santra, N. V. Kryzhevoi, and L. S. Cederbaum, Physical Review Letters **103**, 013002 (2009).

[4] M. H. Chen, Physical Review A **44**, 239 (1991).

[5] B. Rudek, S.-K. Son, L. Foucar, S. W. Epp, B. Erk, R. Hartmann, M. Adolph, R. Andritschke, A. Aquila, N. Berrah, *et al.*, Nature Photonics **6**, 858 (2012).

[6] G. Doumy, C. Roedig, S.-K. Son, C. I. Blaga, A. D. DiChiara, R. Santra, N. Berrah, C. Bostedt, J. D. Bozek, P. H. Bucksbaum, *et al.*, Physical Review Letters **106**, 083002 (2011).

[7] L. J. Frasinski, V. Zhaunerchyk, M. Mucke, R. J. Squibb, M. Siano, J. H. D. Eland, P. Linusson, P. Vd Meulen, P. Salén, R. D. Thomas, *et al.*, Physical Review Letters **111**, 073002 (2013).

[8] S.-K. Son, L. Young, R. Santra, *et al.*, Physical Review A **83**, 033402 (2011).

[9] P. J. Ho, C. Bostedt, S. Schorb, and L. Young, Physical Review Letters **113**, 253001 (2014).

[10] L. Fang, M. Hoener, O. Gessner, F. Tarantelli, S. T. Pratt, O. Kornilov, C. Buth, M. Gühr, E. P. Kanter, C. Bostedt, *et al.*, Physical Review Letters **105**, 083005 (2010).

[11] N. Berrah, L. Fang, B. Murphy, T. Osipov, K. Ueda, E. Kukk, R. Feifel, P. van der Meulen, P. Salén, H. T. Schmidt, *et al.*, Proceedings of the National Academy of Sciences **108**, 16912 (2011).

[12] P. Salén, P. van der Meulen, H. T. Schmidt, R. D. Thomas, M. Larsson, R. Feifel, M. N. Piancastelli, L. Fang, B. Murphy, T. Osipov, *et al.*, Physical Review Letters **108**, 153003 (2012).

[13] M. Larsson, P. Salén, P. van der Meulen, H. T. Schmidt, R. D. Thomas, R. Feifel, M. N. Piancastelli, L. Fang, B. F. Murphy, T. Osipov, *et al.*, Journal of Physics B: Atomic, Molecular and Optical Physics **46**, 164030 (2013).

[14] M. Mucke, V. Zhaunerchyk, L. J. Frasinski, R. J. Squibb, M. Siano, J. H. D. Eland, P. Linusson, P. Salén, P. van der Meulen, R. D. Thomas, *et al.*, New Journal of Physics **17**, 073002 (2015).

[15] M. Hoener, L. Fang, O. Kornilov, O. Gessner, S. T. Pratt, M. Gühr, E. P. Kanter, C. Blaga, C. Bostedt, J. D. Bozek, *et al.*, Physical Review Letters **104**, 253002 (2010).

[16] J. P. Cryan, J. M. Glownia, J. Andreasson, A. Belkacem, N. Berrah, C. I. Blaga, C. Bostedt, J. Bozek, C. Buth, L. F. DiMauro, *et al.*, Physical Review Letters **105**, 083004 (2010).

[17] P. Lablanquie, F. Penent, J. Palaudoux, L. Andric, P. Selles, S. Carniato, K. Bučar, M. Žitnik, M. Huttula, J. H. D. Eland, *et al.*, Physical Review Letters **106**, 063003 (2011).

[18] P. Lablanquie, T. P. Grozdanov, M. Žitnik, S. Carniato, P. Selles, L. Andric, J. Palaudoux, F. Penent, H. Iwayama, E. Shigemasa, *et al.*, Physical Review Letters **107**, 193004 (2011).

[19] J. H. D. Eland, M. Tashiro, P. Linusson, M. Ehara, K. Ueda, and R. Feifel, Physical Review Letters **105**, 213005 (2010).

[20] L. S. Cederbaum, F. Tarantelli, A. Sgamellotti, and J. Schirmer, The Journal of Chemical Physics **85**, 6513 (1986).

[21] E. M.-L. Ohrendorf, L. S. Cederbaum, and F. Tarantelli, Physical Review A **44**, 205 (1991).

[22] N. V. Kryzhevoi, R. Santra, and L. S. Cederbaum, The Journal of Chemical Physics **135**, 084302 (2011).

[23] L. S. Cederbaum, Physical Review A **35**, 622 (1987).

[24] M. Tashiro, M. Ehara, H. Fukuzawa, K. Ueda, C. Buth, N. V. Kryzhevoi, and L. S. Cederbaum, The Journal of Chemical Physics **132**, 184302 (2010).

[25] M. Tashiro, M. Ehara, and K. Ueda, Chemical Physics Letters **496**, 217 (2010).

[26] O. Takahashi, M. Tashiro, M. Ehara, K. Yamasaki, and K. Ueda, Chemical Physics **384**, 28 (2011).

[27] K. Ueda and O. Takahashi, Journal of Electron Spectroscopy and Related Phenomena **185**, 301 (2012).

[28] M. Nakano, F. Penent, M. Tashiro, T. P. Grozdanov, M. Žitnik, S. Carniato, P. Selles, L. Andric, P. Lablanquie, J. Palaudoux, *et al.*, Physical Review Letters **110**, 163001 (2013).

[29] S. Carniato, P. Selles, L. Andric, J. Palaudoux, F. Penent, M. Žitnik, K. Bučar, M. Nakano, Y. Hikosaka, K. Ito, *et al.*, The Journal of Chemical Physics **142**, 014307 (2015).

[30] S. Carniato, P. Selles, L. Andric, J. Palaudoux, F. Penent, M. Žitnik, K. Bučar, M. Nakano, Y. Hikosaka, K. Ito, *et al.*, The Journal of Chemical Physics **142**, 014308 (2015).

[31] C. Buth, J.-C. Liu, M. H. Chen, J. P. Cryan, L. Fang, J. M. Glownia, M. Hoener, R. N. Coffee, and N. Berrah, The Journal of Chemical Physics **136**, 214310 (2012).

[32] S.-K. Son, R. Santra, *et al.*, Physical Review A **85**, 063415 (2012).

[33] L. Inhester, K. Hanasaki, Y. Hao, S.-K. Son, R. Santra, *et al.*, Physical Review A **94**, 023422 (2016).

[34] L. Inhester, C. F. Burmeister, G. Groenhof, and H. Grubmueller, The Journal of Chemical Physics **136**, 144304 (2012).

[35] N. Berrah and L. Fang, Journal of Electron Spectroscopy and Related Phenomena **204**, 284 (2015).

[36] M. Tashiro, K. Ueda, and M. Ehara, Chemical Physics Letters **521**, 45 (2012).

[37] E. Pahl, H.-D. Meyer, and L. S. Cederbaum, Zeitschrift für Physik D Atoms, Molecules and Clusters **38**, 215 (1996).

[38] J. Stöhr, *NEXAFS spectroscopy*, Vol. **25** (Springer Science & Business Media, 2013).

[39] B. H. Bransden and C. J. Joachain, *Quantum mechanics* (Pearson Education, 2000).

[40] P. V. Demekhin and L. S. Cederbaum, Physical Review A **83**, 023422 (2011).

[41] F. F. Guimarães, *X-ray Spectroscopy of Molecules Driven by Strong IR Fields*, Ph.D. thesis (2006).

[42] T. H. Dunning Jr., The Journal of Chemical Physics **90**, 1007 (1989).

[43] C. Nicolas and C. Miron, Journal of Electron Spectroscopy and Related Phenomena **185**, 267 (2012).

[44] T. X. Carroll, K. J. Børve, L. J. Sæthre, J. D. Bozek, E. Kukk, J. A. Hahne, and T. D. Thomas, The Journal of Chemical Physics **16**, 10221 (2002).

[45] M. Coville and T. D. Thomas, Physical Review A **43**, 6053 (1991).

[46] F. P. Larkins, Australian Journal of Physics **49**, 457 (1996).

[47] L. J. Medhurst, P. A. Heimann, M. R. F. Siggel, D. A. Shirley, C. T. Chen, Y. Ma, S. Modesti, and F. Sette, Chemical Physics Letters **193**, 493 (1992).

[48] K. J. Randall, A. L. D. Kilcoyne, H. M. Köppe, J. Feldhaus, A. M. Bradshaw, J.-E. Rubensson, W. Eberhardt, Z. Xu, P. D. Johnson, and Y. Ma, Physical Review Letters **71**, 1156 (1993).

[49] S. J. Osborne, A. Ausmees, S. Svensson, A. Kivimäki, O.-P. Sairanen, A. N. de Brito, H. Aksela, and S. Aksela, The Journal of Chemical Physics **102**, 7317 (1995).

[50] H. M. Köppe, A. L. D. Kilcoyne, J. Feldhaus, and A. M. Bradshaw, Journal of Electron Spectroscopy and Related Phenomena **75**, 97 (1995).

[51] U. Hergenhahn, Journal of Physics B: Atomic, Molecular and Optical Physics **37**, R89 (2004).

[52] L. Inhester, G. Groenhof, and H. Grubmüller, The Journal of Chemical Physics **138**, 164304 (2013).

[53] M. H. Beck, A. Jäckle, G. A. Worth, and H.-D. Meyer, "The multiconfiguration time-dependent hartree (MCTDH) method: A highly efficient algorithm for propagating wavepackets," Elsevier (2012).

[54] W. H. Press, B. P. Flannery, S. A. Teukolsky, and W. T. Vetterling, *Numerical Recipes (FORTRAN Version) Cambridge University Press* (Press Syndicate of the University of Cambridge, New York, USA, 1989).